Eur. Phys. J. B **41**, 67–74 (2004)
DOI: 10.1140/epjb/e2004-00295-5

THE EUROPEAN PHYSICAL JOURNAL B

Exact solution and magnetic properties of an anisotropic spin ladder

Zu-Jian Ying[1,2,3,a], Itzhak Roditi[1], Angela Foerster[3], and Bin Chen[2]

[1] Centro Brasileiro de Pesquisas Físicas, Rua Dr. Xavier Sigaud 150, 22290-180 Rio de Janeiro, RJ, Brasil
[2] Department of Physics, Hangzhou Teachers College, Hangzhou 310012, P.R. China
[3] Instituto de Física da UFRGS, Av. Bento Gonçalves 9500, Porto Alegre, 91501-970, Brasil

Received 20 March 2004 / Received in final form 21 May 2004
Published online 30 September 2004

Abstract. We study an integrable two-leg spin-1/2 ladder with an XYZ-type rung interaction. The exact rung states and rung energies are obtained for the anisotropic rung coupling in the presence of a magnetic field. The magnetic properties are analyzed at both zero and finite temperatures via the thermodynamic Bethe ansatz and the high-temperature expansion. According to different couplings in the anisotropic rung interaction, there are two cases in which a gap opens, where the ground state involves one or two components in the absence of a magnetic field. We obtain the analytic expressions of all critical fields for the field-induced quantum phase transitions (QPT). The anisotropic rung interaction leads to such effects as separated magnetizations and susceptibilities in different directions, lowered inflection points, and remnant weak variation of the magnetization after the last QPT.

PACS. 75.10.Jm Quantized spin models – 75.30.Kz Magnetic phase boundaries (including magnetic transitions, metamagnetism, etc.) – 75.40.Cx Static properties (order parameter, static susceptibility, heat capacities, critical exponents, etc.)

1 Introduction

Recently the quasi-one-dimensional spin ladder has attracted much interest, both experimentally and theoretically [1]. More and more ladder-structure compounds have been realized, such as $SrCu_2O_3$ [2], $Cu_2(C_5H_{12}N_2)_2Cl_4$ [3], $(5IAP)_2CuBr_4{\cdot}2H_2O$ [4], $(C_5H_{12}N)_2CuBr_4$ [5], and so forth. Although many ladder compounds can be well described by simple isotropic ladders, the structural distortion and the spin-orbit interaction of the transition ions can lead to various magnetic anisotropies. Besides the spin-orbit interaction, both the on-site Coulomb exchange interaction [6,7] and the nonlocal Coulomb interaction [8] can also influence the anisotropy. The anisotropic interaction from bond buckling has been recently found in copper-oxide ladder compounds $CaCu_2O_3$ [9] due to an angle deviation from 180° in the Cu-O-Cu bond [9–11]. An anisotropic rung interaction was considered in references [12,13] motivated by $CaCu_2O_3$ [9], and a two-leg spin ladder with an XXZ-rung interaction was derived in the presence of the Dzyaloshinskii-Moriya interaction and the Kaplan-Shekhtman-Entin- Wohlman-Aharony interactions. When the Cu-O-Cu bond is near 90°, the rung interaction is weak in the copper-oxide ladder. Spin anisotropy in the exchange interaction also exists in strongly-coupled ladder compounds such as $(pipdH)_2CuBr_4$ [14]. On the other hand, real spin ladder compounds are usually described by the standard Heisenberg ladder model, which is not exactly soluble, thus turning the computation of the physical properties for the ground state (GS), the gap, the thermodynamical quantities and other relevant properties in the presence of temperature and magnetic fields, rather difficult. The theoretical methods that are usually applied are numerical ones [15–17], as well as perturbation expansions [18], bosonization [19] and mapping into the XXZ Heisenberg chain [20] in strong-coupling limit. Recently it was shown that the integrable isotropic spin ladder model [21] can be used to describe the properties of strongly-coupled spin ladder compounds [22–24]. Therefore, it can be expected that integrable ladders with anisotropic rung interactions can provide some meaningful information about the physics of anisotropies. The bulk leg part of the two-leg spin-1/2 integrable spin ladder [21] is the SU(4) model [25,26]. For the spin-orbit system, various breakings of the SU(4) symmetry were analyzed in the presence of detailed phase diagrams [27], together with some interesting five-consecutive field-induced quantum phase transitions (QPT), as well as magnetization plateaus arising from different Landé g factors and the one-site anisotropy, as revealed in a globally-analytic phase diagram [28]. For the ladder case, the XXZ anisotropic rung interaction in

[a] e-mail: ying@cbpf.br

the presence of an external field in the z-direction was embedded in the SU(4) bulk leg part in reference [13], and some phase diagrams for the GS were obtained. For a more general XYZ anisotropic rung interaction, new physics can be expected as the additional anisotropy in the x- and y-directions from the XYZ rung coupling will break the linear field dependence of the Zeeman energy in the isotropic or XXZ anisotropic case. To our knowledge, the explicit solutions in different anisotropic directions, in the absence and presence of the field, field-induced QPT's and the detailed magnetic properties for the GS and at finite temperatures, have not yet been addressed for the general XYZ anisotropic case.

In the present paper we shall consider the anisotropy in the rung interaction and the corresponding magnetic anisotropy effect by solving an integrable spin ladder with a general XYZ rung interaction. By means of the thermodynamical Bethe ansatz (TBA) [23,26–30] and the high temperature expansion (HTE) [22,31,32], we investigate the influence of the anisotropic rung interaction on the QPT's and the magnetic properties. The contents are arranged as follows: (i) in Section 2 we present the model and the exact rung-state basis in the presence of a magnetic field. The model is then solved by the Bethe ansatz (BA) approach. (ii) Section 3 gives the TBA equations for the GS and the HTE of the physical properties at finite temperatures. (iii) In Section 4, we study the field-induced QPT's. The rung anisotropy provides two kinds of gapped ladders, with one and two components in the GS. The analytic expressions are obtained for all the critical fields of the corresponding QPT's. The rung anisotropy also leads to a separation of the magnetizations and susceptibilities in different directions. The magnetization inflection point (IP) may be lowered from the half-saturation, and in the two-component gapped ladder, the IP is not even invariant under different temperatures. A remnant variation of magnetization can be found after the last QPT. In Section 5 we give a summary of our results.

2 The model, exact rung states and BA solution

We shall consider a spin-1/2 two-leg spin ladder model with a general XYZ-type anisotropy in the rung interaction, whose Hamiltonian reads

$$\begin{aligned}\mathcal{H} &= \mathcal{H}_0 + \mathcal{H}_{XYZ} + \mathcal{M},\\ \mathcal{H}_0 &= J_0 \sum_{i=1}^{L} P_{i,i+1},\\ \mathcal{H}_{XYZ} &= \sum_i (J_x S_i^x T_i^x + J_y S_i^y T_i^y + J_z S_i^z T_i^z),\\ \mathcal{M} &= -gH \sum_i (S_i^z + T_i^z),\end{aligned} \tag{1}$$

where $\boldsymbol{S}$ and $\boldsymbol{T}$ are the spin operators for the two legs, and g is the Landé g factor in the direction of the field. The bulk part $\mathcal{H}_0$ with the permutation operator $P_{i,i+1} = (2\boldsymbol{S}_i \cdot \boldsymbol{S}_{i+1} + \frac{1}{2})(2\boldsymbol{T}_i \cdot \boldsymbol{T}_{i+1} + \frac{1}{2})$, exhibits the SU(4) symmetry [25]. Isotropic integrable spin ladders [21] have identical rung interactions $J_x = J_y = J_z = J$. For real spin ladder compounds, we shall denote the real average leg interaction by $J_\parallel$, and the anisotropic rung interactions by $J_\perp^x$, $J_\perp^y$, $J_\perp^z$. For the isotropic case, a scaling parameter $\gamma \approx 4$ in the leg interaction $J_0 = J_\parallel/\gamma$ fits the leading terms of the gap [23] for strong-coupling spin ladders in the presence of a weak rung interaction. Another set of parameters ($J_0 = J_\parallel/\gamma$, $J = J_\perp + \alpha J_\parallel$) were introduced, and by minimizing the effect of the biquadratic leg interaction, the deduced parameters $\gamma \approx 8/3, \alpha \approx 1/2$ give the leading terms of both the gap and the fully-polarized critical point of real compounds [24]. In the discussed anisotropic case, defining

$$J_0 = J_\parallel/\gamma,\ J_\nu = J_\perp^\nu + \alpha_\nu J_\parallel\ (\nu = x, y, z) \tag{2}$$

with adjustable γ and α_ν may also be helpful in understanding real compounds. In the present paper we shall discuss the general solution and effect of the anisotropic J_ν.

When the rung interaction is strong, it is favorable for the spin ladder system to form rung states since the leg interaction is too weak to take apart the rung states. Anisotropy in the rung interaction leads to the collapse of the conventional singlet and triplet rung states from the isotropic ladder, even in the absence of the field. However, we find a new exact basis, valid both in the absence and presence of an external magnetic field as such:

$$\begin{aligned}&\varphi_1 = \frac{1}{\sqrt{2}}(|\uparrow\downarrow\rangle - |\downarrow\uparrow\rangle) \quad \varphi_2 = \frac{1}{\sqrt{2}}(|\uparrow\downarrow\rangle + |\downarrow\uparrow\rangle)\\ &\varphi_3 = \frac{|\uparrow\uparrow\rangle - \eta^{-1}|\downarrow\downarrow\rangle}{\sqrt{1+\eta^{-2}}} \quad \varphi_4 = \frac{|\uparrow\uparrow\rangle + \eta|\downarrow\downarrow\rangle}{\sqrt{1+\eta^2}},\end{aligned} \tag{3}$$

where

$$\eta^{\pm 1} = \frac{\pm 4gH + \sqrt{(4gH)^2 + (J_x - J_y)^2}}{J_x - J_y}. \tag{4}$$

The corresponding rung energies then include the Zeeman energy in a nonlinear way,

$$\begin{aligned}E_1 &= -\frac{1}{4}(J_x + J_y + J_z),\\ E_2 &= \frac{1}{4}(J_x + J_y - J_z),\\ E_3 &= -\sqrt{(gH)^2 + \frac{1}{16}(J_x - J_y)^2} + \frac{1}{4}J_z,\\ E_4 &= \sqrt{(gH)^2 + \frac{1}{16}(J_x - J_y)^2} + \frac{1}{4}J_z.\end{aligned} \tag{5}$$

The rung states $\{\varphi_i \mid i = 1, \cdots, 4\}$ provide a new fundamental representation of the SU(4) Lie algebra $S_m^n \varphi_i = \delta_{n,i}\varphi_m$, with commutation relations of the generators $[S_m^n, S_k^l] = \delta_{n,k}S_m^l - \delta_{m,l}S_k^n$. Based on this SU(4) realization and the vanishing commutation relations $[\mathcal{H}_{XYZ}, \mathcal{H}_0] = [\mathcal{M}, \mathcal{H}_0] = 0$, one can solve the

model (1) via the BA approach [33]. The BA equations are the same as those obtained for the SU(4) model [26] and for the SU(3)⊗U(1) spin ladder [21]. Here we present the BA equations together with the eigenenergy

$$-\prod_{m=1}^{M^{(k)}}\Xi_1(\mu_{j,m}^{k,k})=\prod_{m=1}^{M^{(k+1)}}\Xi_{\frac{1}{2}}(\mu_{j,m}^{k,k+1})\prod_{m=1}^{M^{(k-1)}}\Xi_{\frac{1}{2}}(\mu_{j,m}^{k,k-1}),$$

$$E=-J_0\sum_{j=1}^{M^{(1)}}2\pi a_1(\mu_j^{(1)})+\sum_{i=1}^{4}E_iN_i, \quad (6)$$

where $\Xi_x(\mu_{j,m}^{k,l})=(\mu_j^{(k)}-\mu_m^{(l)}-xi)/(\mu_j^{(k)}-\mu_m^{(l)}+xi)$, $\mu_j^{(0)}=0, M^{(0)}=L, M^{(4)}=0$, and $1\le k\le 3$; $a_n(\mu)=[n/(\mu^2+n^2/4)]/(2\pi)$. There are L rungs, N_i is the total number of rung states φ_i, and $\mu_j^{(k)}$ is the rapidity. $M^{(k)}$ is the total rapidity number in the k'th branch.

From the BA equations and the eigenenergy we can apply the TBA and HTE to study the collective properties of the model. When the field is applied in the x- or y-direction, one only needs to permute the anisotropy parameter values $\{J_x, J_y, J_z\}$ as well as the corresponding g factors. We incorporate g into the field unit when plotting figures in order to investigate the net effect of the anisotropic rung interaction. For a powder sample, one simply takes an average over the three directions.

3 TBA and HTE

By adopting the string conjectures [34] and by applying the Yang-Yang method [29] at the thermodynamic limit, one can obtain the GS equations for three dressed energies $\epsilon^{(i)}$ [23,27,28,30],

$$\epsilon^{(i)}=g^{(i)}-a_2*\epsilon^{(i)-}+a_1*\left(\epsilon^{(i-1)-}+\epsilon^{(i+1)-}\right), \quad (7)$$

where $\epsilon^{(0)}=\epsilon^{(4)}=0$ and the symbol $*$ denotes the convolution. The basis order is chosen as $(\varphi_{P_1}\varphi_{P_2}\varphi_{P_3}\varphi_{P_4})^T$, where $P_i\in\{1,2,3,4\}$, and φ_{P_1} is energetically the most favorable state, while φ_{P_4} is the least favorable one. For the chosen order, the driving term is given by $g^{(i)}=(E_{P_{i+1}}-E_{P_i})/J_0-\delta_{i,1}2\pi a_1$. The GS is composed of Fermi seas filled by negative $\epsilon^{(i)-}$. If some branch of the dressed energy is all positive, then the corresponding excitations to this branch is gapped. A QPT occurs at the point where the gap is closed. We shall apply these TBA equations to analyze the field-induced QPT for the GS.

For the finite temperature case the TBA involves an infinite number of coupled integral equations. In the present paper we shall apply the HTE [22,31,32] from T-system [35] within the Quantum Transfer Matrix formalism [36], which involves only a finite number of integral equations, and consequently is more convenient. Following references [22,31,32], one can obtain the free energy f per rung at high temperatures. Here we present the first four terms which dominate the physics for high temperatures:

$$f=-T\left(C_0+C_1\left(\frac{J_0}{T}\right)+C_2\left(\frac{J_0}{T}\right)^2+C_3\left(\frac{J_0}{T}\right)^3\right) \quad (8)$$

where T is the temperature, and the coefficients are

$$C_0=\ln Q_+,\ C_1=\frac{2Q}{Q_+^2},\ C_2=\frac{3Q}{Q_+^2}-\frac{6Q^2}{Q_+^4}+\frac{3Q_-}{Q_+^3},$$

$$C_3=\frac{10Q}{3Q_+^2}-\frac{18Q^2}{Q_+^4}+\frac{80Q^3}{3Q_+^6}+\frac{8Q_-}{Q_+^3}-\frac{24QQ_-}{Q_+^5}+\frac{4}{Q_+^4},$$

with the following definitions

$$Q=2\cosh\left(\frac{1}{2}\beta J_z\right)+4\cosh\left(\frac{1}{4}\beta J_{x+y}\right)\cosh(\beta h),$$

$$Q_\pm=2e^{(\pm\beta J_z/4)}\cosh\left(\frac{1}{4}\beta J_{x+y}\right)+2e^{(\mp\beta J_z/4)}\cosh(\beta h),$$

$h=\sqrt{(gH)^2+{J_{x-y}}^2/16}$, $J_{x\pm y}=J_x\pm J_y$ and $\beta=1/T$. One can get higher orders for lower temperatures. The magnetization and the susceptibility can be easily obtained by $M=-\partial f/\partial H$, $\chi=\partial M/\partial H$. If the rung J_0 is weak, then the HTE gives a valid result even for low temperatures due to the large rescaling γ. In the isotropic case, $\gamma=4$ [23] fits the leading order terms of the gap, while $\gamma=5$ was also used in reference [22] for fitting some compound. In reference [24], $\gamma\approx 8/3$ together with a new parameter $\alpha=1/2$ were determined by minimizing the effect of the biquadratic leg interaction.

4 Phase transitions and magnetic properties

4.1 One-component gapped ladder

For different anisotropies, there are two different gapped ladders. In one case, only one component φ_1 exists in the gapped GS when $H=0$. In the other case, both φ_1 and φ_2 are involved in the gapped GS. First we discuss the former case which happens to be more likely. It requires that

$$J_z+J_3-|J_x-J_y|>16J_0, \quad (9)$$

$$J_x+J_y>8J_0, \quad (10)$$

where $J_3=J_x+J_y+J_z$. Condition (9) expels the components φ_3 and φ_4 from the GS, while condition (10) excludes the component φ_2. The field will bring φ_3 down to the ground state and close the gap $\Delta=\min\{E_2,E_3,E_4\}-E_1-4J_0$ at a critical field H_{c1}, which leads to the first QPT. Further increase of the field will bring all components of φ_1 out of the GS and another gap $\Delta=E_1-E_3-4J_0$ opens at the critical field H_{c2}, which characterizes another QPT. The factor $4J_0$ in the gap comes from the maximum depth of the first dressed energy branch. It is easy to see that only the components φ_1 and φ_3 compete in the GS (which involves one branch of the dressed

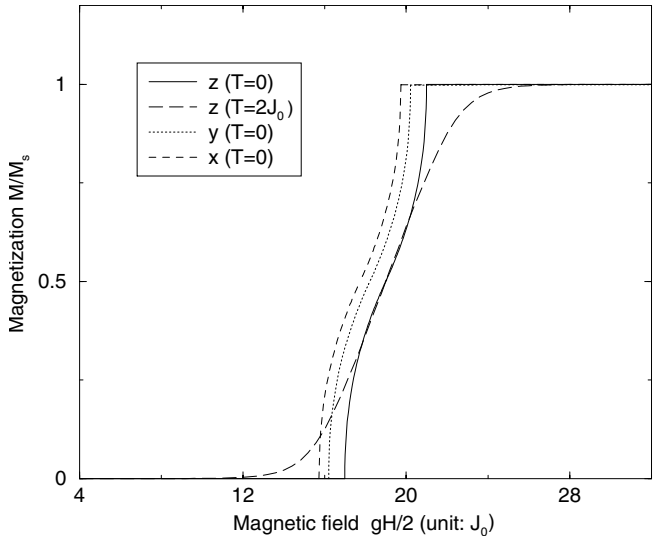

Fig. 1. Magnetization versus magnetic field at zero temperature for the one-component gapped ladder with a weakly-anisotropic rung interaction, $J_x = 32J_0$, $J_y = 36J_0$, $J_z = 42J_0$. From the rescaling $\gamma \approx 4$ [23] or $\gamma \approx 8/3, \alpha \approx 1/2$ [24] in (2), the ratio of real leg ($J_\parallel$) and rung ($J_\perp$) couplings for compounds will be of the order $J_\parallel/J_\perp \sim 0.1$. M_s is the saturation magnetization. In the gapped phase $H < H_{c1}$, only one component, φ_1, exists in the ground state. In order to study the net effect of the anisotropic rung interaction, we incorporate the g factor into the field. The weak anisotropy in the rung separates the magnetization in different directions. The zero temperature magnetization is obtained from the thermodynamic Bethe ansatz (TBA). Also, for comparison with the finite temperature case, a magnetization at $T = 2J_0$ obtained from the high-temperature expansion (HTE) is presented in the z-direction.

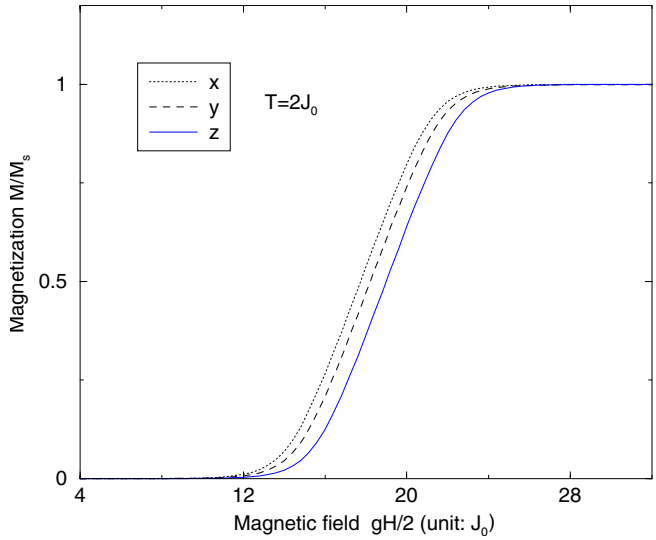

Fig. 2. Magnetization versus magnetic field for $T = 2J_0$ for the one-component gapped ladder with the weak anisotropy, $J_x = 32J_0$, $J_y = 36J_0$, $J_z = 42J_0$. The magnetizations are obtained from the HTE, which coincides with the magnetization separation in the zero temperature case obtained from the TBA.

energy), since the GS only consists of φ_1 in the absence of the field, while only φ_3 is lowered in energy when the field is applied. The analytic expressions of two critical fields can be obtained exactly as

$$H_{c1} = \frac{1}{2g}\sqrt{J_zJ_3 + J_xJ_y + 64J_0^2 - 8J_0\,(J_z + J_3)},$$
$$H_{c2} = \frac{1}{2g}\sqrt{J_zJ_3 + J_xJ_y + 64J_0^2 + 8J_0\,(J_z + J_3)}. \quad (11)$$

In the above expressions, setting $J_\perp^\nu = J_\perp$ and $\gamma = 8/3$, $\alpha_\nu = 1/2$ (for all $\nu = x, y, z$) from (2) recovers the result of isotropic case in reference [24] with the two critical fields $gH_{c1} = J_\perp - J_\parallel$ and $gH_{c2} = J_\perp + 2J_\parallel$, which are the leading terms of the two critical fields of the isotropic spin ladder compounds [3,20,37–39]. A weak anisotropy will lead to different critical fields and consequently separate the magnetizations in different directions. We give an example of the magnetization with weak anisotropy in Figure 1 (a low-temperature magnetization is presented for comparison in the z-direction). The corresponding low-temperature magnetizations for all three directions are presented in Figure 2, as obtained from the HTE. As an example, magnetizations in different directions for strong anisotropy are shown in Figure 3 for the GS and in Figure 4 for a low temperature.

Before the gap is closed at H_{c1}, the gap Δ near H_{c1} can be expanded to a simpler form

$$\Delta \cong c_1\,(H_{c1} - H)\,, \quad (12)$$

where $c_1 = g^2H_{c1}/\sqrt{(gH_{c1})^2 + \frac{1}{16}(J_x - J_y)^2}$. Considerable excitations can be stimulated by the temperature T if T is of the order of the gap $T \sim (H_{c1} - H)$, and the magnetization will rise from zero before the field reaches the critical point. An expansion based on small Fermi points [23] gives the zero-temperature critical behavior in the vicinity of H_{c1}

$$\langle M^z\rangle \cong \langle M^z\rangle_3 \frac{1}{\pi}\sqrt{\frac{c_1}{J_0}}(H - H_{c1})^{1/2}. \quad (13)$$

Here $\langle M^z\rangle_3$ is the magnetization of a single rung state φ_3, which also varies with the field due to the anisotropic rung interaction, as we will discuss below in (18). For the lowest order in the critical behavior, $\langle M^z\rangle_3$ takes the value at the critical point H_{c1}. This $M^z \propto (H - H_{c1})^{1/2}$ critical behavior, typical for gapped integer spin antiferromagnetic chains [40], is buried by the afore-mentioned temperature effect. This temperature effect can be seen in Figure 5, where the magnetization along the z-direction at $T = 2J_0$ becomes considerable at the field $H = H_{c1} - 2J_0$. Actually, the magnetization at $T = 2J_0$ increases almost linearly before H_{c1}.

A special point in the magnetization is the inflection point (IP) H_{IP}, which is an invariant point at low temperatures, given by

$$gH_{IP} = \frac{1}{2}\sqrt{(J_z + J_x)(J_z + J_y)}, \quad (14)$$

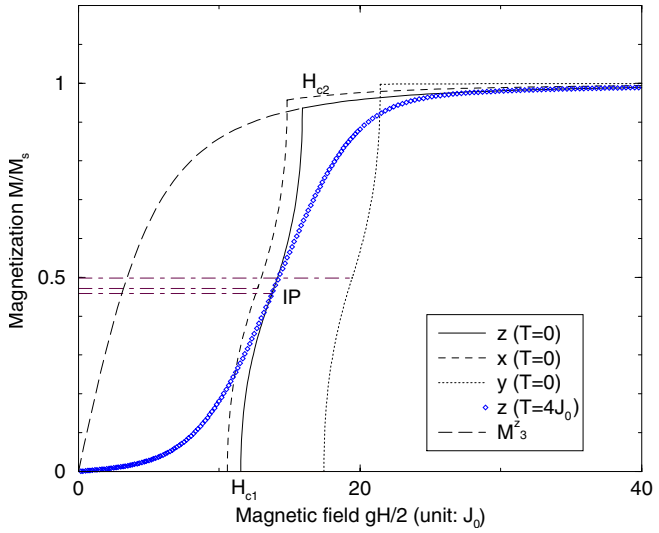

Fig. 3. Magnetization versus magnetic field at zero temperature for the one-component gapped ladder with a strongly-anisotropic rung interaction, $J_x = 12J_0$, $J_y = 60J_0$, $J_z = 24J_0$. The strong anisotropy leads to a strong separation of the magnetization. The inflection point (IP) is lowered from the half saturation. A finite temperature magnetization from HTE is presented in order to demonstrate the IP. Note that the magnetizations do not reach the saturation after the second quantum phase transition at H_{c2}, and there still remains a weak variation of the magnetizations. This remnant magnetization variation comes from the single-state magnetization M_3^z of φ_3 which is a mixture of full-polarized states $|\uparrow\uparrow\rangle$ and the lowest-magnetized state $|\downarrow\downarrow\rangle$. The variation of M_3^z is illustrated by the long-dashed line for the whole process of the field application.

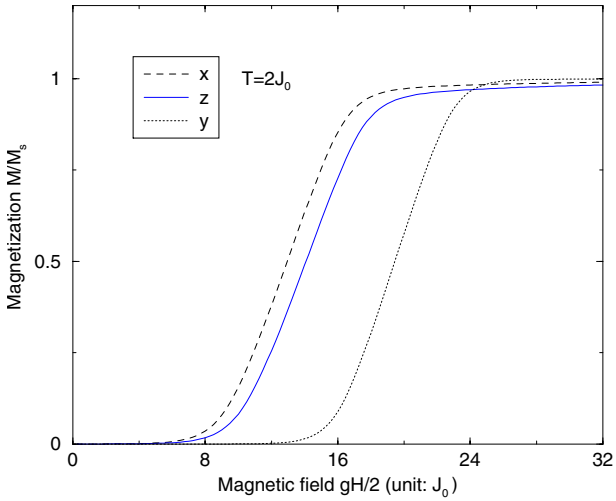

Fig. 4. Magnetizations versus magnetic field for different directions at finite temperature for the one-component gapped ladder with the strong anisotropy, $J_x = 12J_0$, $J_y = 60J_0$, $J_z = 24J_0$.

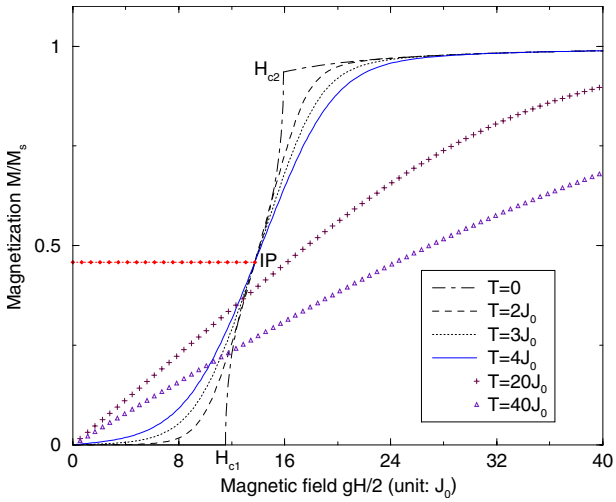

Fig. 5. Magnetization versus magnetic field at different temperatures for the strongly-anisotropic rung, $J_x = 12J_0$, $J_y = 60J_0$, $J_z = 24J_0$. Low temperature magnetizations at $T = 0$, $2J_0$, $3J_0$ and $4J_0$ cross the inflection point (IP). Higher-temperature magnetizations at $T = 20J_0$ and $40J_0$ do not go through the IP, since the gap of excitation for φ_2 is overcome by the temperature stimulation.

where the two components φ_1 and φ_3 have the same rung energies $E_1 = E_3$ and the same proportion $N_1 = N_3$ in the GS. The excitations for φ_2 and φ_4 are gapped, and the gap can be obtained exactly from (7), giving

$$\begin{aligned} \Delta_{IP} &= \min\{\Delta_{IP2}, \quad \Delta_{IP4}\}, \\ \Delta_{IP2} &= (J_x + J_y)/2 - (2\ln 2)J_0, \\ \Delta_{IP4} &= (J_z + J_3)/2 - (2\ln 2)J_0. \end{aligned} \tag{15}$$

At low temperatures, the excitations for φ_2 or φ_4 are difficult to stimulate, while the temperature does not influence the relative proportion between φ_1 and φ_3 due to their similar energies at the IP. Consequently the proportions of φ_1 and φ_3 remain almost unchanged when the temperature varies. Therefore the magnetization at H_{IP} also remains invariant when the temperatures changes, and the magnetization curves at various temperatures cross each other at the same point M_{IP}, as shown by the curves for temperatures $T = 0$, $2J_0$, $3J_0$ and $4J_0$ in Figure 5. This requires low temperatures

$$T \ll \Delta_{IP}, \tag{16}$$

as well as the gapped ladder conditions (9) and (10), where Δ_{IP} is the excitation gap for φ_2 or φ_4 in (15). When the temperature is sufficiently high such that the excitations to φ_2 or φ_4 are considerable, the involvement of these components reduces the proportion of φ_3 which has the highest magnetization. The components φ_2 and φ_4 have zero and negative magnetizations, respectively. As a result, the magnetization at H_{IP} deviates from M_{IP} and move downwards. We show this motion by using the magnetization curves at temperatures $T = 20J_0$, $40J_0$ in Figure 5, for which one can compare with observation examples such as $Cu_2(C_5H_{12}N_2)_2Cl_4$ [3], and also from the TMRG numerical result for the Heisenberg ladder [16].

The magnetization at the IP can be worked out as follows

$$M^z_{IP} = \frac{g}{2}\frac{{H_{IP}}^2 + H_{IP}H^{(+)}_{IP}}{H^{(+)2}_{IP} + H_{IP}H^{(+)}_{IP}}, \tag{17}$$

where $H^{(+)}_{IP} = \sqrt{H^2_{IP} + (J_x - J_y)^2/(4g)^2}$. For the isotropic ladder $H^{(+)}_{IP} = H_{IP}$, and consequently M^z_{IP} is located at the half of the saturation magnetization $M^z_s = g$ [22]. The anisotropy lowers the magnetization of the IP due to the fact that $H^{(+)}_{IP} > H_{IP}$, i.e. $M^z_{IP}/M^z_s < 1/2$. Physically, the anisotropy in the x,y-directions hybridizes the elemental state $|\downarrow\downarrow\rangle$ into φ_3 such that φ_3 is not a pure fully-polarized elemental state $|\uparrow\uparrow\rangle$ as in the isotropic case. For the XXZ-type rung interaction, M^z_{IP} is half-saturated when the field is oriented in the z-direction, while lowered when the field is applied in other directions. This IP lowering effect is more obvious for the strong anisotropic case, we give an example in Figure 3. As one can see from this figure, besides the strong separation of the magnetization in different directions, the IP points in the x- and z-directions move below the half saturation point.

In addition to the separation of the magnetizations in different directions, and the lowering of the inflection points, another property in the anisotropic case is the remnant variation of the magnetization after the second phase transition. The fact that the magnetization increases between H_{c1} and H_{c2} comes mainly from the proportional competition between the two state φ_1 and φ_3, i.e., more rungs are occupied by φ_3 when the field increases. The single-rung magnetization in state φ_3 can be obtained explicitly as

$$\langle M^z\rangle_3 = g\frac{\eta^2 - 1}{\eta^2 + 1}, \tag{18}$$

where η increases with the field according to the expression (4). The long-dashed line in Figure 3 gives an example of $\langle M^z\rangle_3$ in the z direction, which increases from zero at the beginning of the application of the magnetic field. If H_{c1} is small, then the increment of $\langle M^z\rangle_3$ also makes an important contribution to the growth of the magnetization. Otherwise, for higher H_{c1}, the change of $\langle M^z\rangle_3$ contributes less to the growth of the total magnetization, since $\langle M^z\rangle_3$ has decelerated before the first quantum phase transition occurs. However, the competition between φ_1 and φ_3 comes to an end after the second QPT, and the magnetization is given completely by $\langle M^z\rangle_3$. This gives a remnant variation of magnetization even after the second QPT, since $\langle M^z\rangle_3$ is still approaching the saturation limit. This remnant variation of the magnetization is illustrated for the GS in Figure 3 and can also be seen for the temperature variant case (Fig. 4).

Examples of the magnetic susceptibility in the three directions are plotted in Figure 6 for weakly anisotropic rungs, and in Figure 7 for strongly anisotropic rungs. Weak anisotropy separates the heights of the magnetic susceptibility peaks, while a strong anisotropy leads to an obvious separation of the whole susceptibility, including the peak positions.

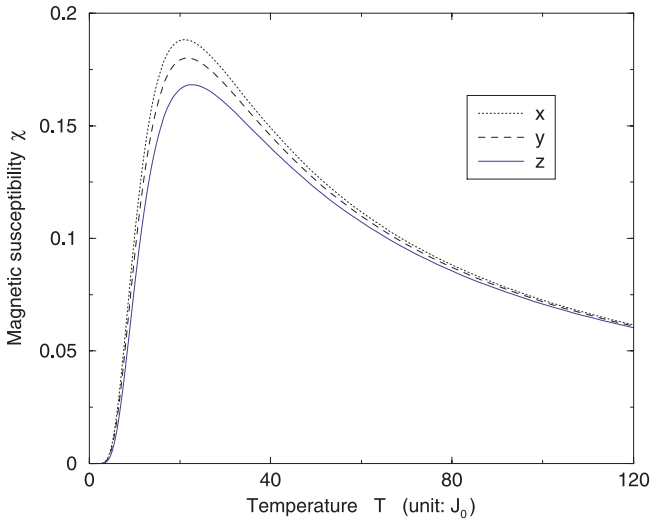

Fig. 6. Magnetic susceptibility against temperature for different directions in the weakly-anisotropic case, $J_x = 32J_0$, $J_y = 36J_0$, $J_z = 42J_0$. The weak anisotropy separates the heights of the susceptibility peaks. In order to see the net effect of the rung anisotropy, we plot the figures using the same g factors for the three directions.

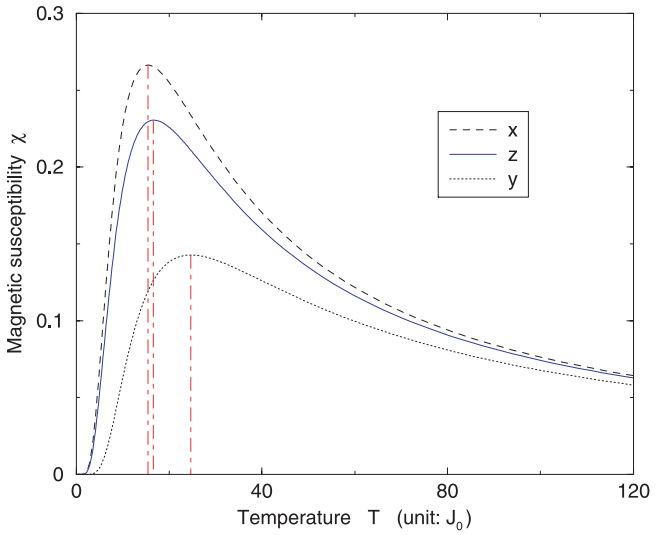

Fig. 7. Magnetic susceptibility versus temperature for the strongly-anisotropic case, $J_x = 12J_0$, $J_y = 60J_0$, $J_z = 24J_0$. The strong anisotropy separates not only the peak heights, but also the whole shape including the peak positions.

4.2 Two-component gapped ladder

The anisotropy in the rung interaction provides another possibility of a gapped ladder, in which not only the rung state φ_1, but also φ_2 are involved in the GS before the field brings about the first QPT. The single-state energy difference is $E_2 - E_1 = (J_x + J_y)/2$. The larger the difference, the more φ_1 and φ_2 expel each other in the Fermi sea. The two-component gapped ladder requires that

$$|J_x + J_y| < 8J_0, \tag{19}$$

such that φ_1 and φ_2 are close enough in energy to exist in the GS at the same time, in the absence of the field. Also, a strong J_z is needed to expel φ_3 and φ_4 from the gapped GS before the field is applied, with the approximate condition that

$$J_z > 4\ln 2 J_0 + \frac{1}{2}|J_x - J_y| + \frac{(J_x+J_y)^2}{8\pi^2 J_0}. \qquad (20)$$

For simplicity, we assume $J_x + J_y > 0$ so that φ_1 has lower energy than φ_2, then one only needs to change $J_x + J_y$ to $-(J_x + J_y)$ for lower φ_2. The first QPT occurs when the field lowers the energy of φ_3 and mixes it in the GS, and the critical field can be obtained with the help of the Wiener-Hopf technique [41] which is valid for large Fermi points (Fermi surface in one dimension). Explicitly we have

$$gH_{c1} \cong \sqrt{\left[\frac{J_z}{2} - 2\ln 2 J_0 - \frac{(J_x+J_y)^2}{16\pi^2 J_0}\right]^2 - \frac{(J_x-J_y)^2}{16}}, \qquad (21)$$

which gives a good approximation if the value of $J_x + J_y$ is not very close to $8J_0$. Further increase of the field will lower the energy of φ_3 below φ_1 and φ_2, and will bring them out of the GS one by one. The component variations in the QPT are $\{\varphi_1, \varphi_2\} \to \{\varphi_1, \varphi_2, \varphi_3\} \to \{\varphi_1, \varphi_3\} \to \{\varphi_3\}$, where each arrow indicates the occurrence of a QPT. Since φ_2 has zero magnetization, the total magnetization also remains null in the gapped phase before the first QPT. The zero-magnetization component φ_2 gets out of the GS after H_{IP} if

$$J_x + J_y < (4\ln 2)J_0, \qquad (22)$$

while for

$$(4\ln 2)J_0 < J_x + J_y < 8J_0, \qquad (23)$$

φ_2 is brought out of the GS before H_{IP}. These happen at the second QPT with an approximate critical field

$$gH_{c2} \cong \sqrt{\left[\frac{1}{2}J_z - \frac{3}{4}J_{x+y} + 4\ln 2 J_0 + \frac{\delta^2}{2\pi^2 J_0}\right]^2 - \frac{J_{x-y}^2}{16}}, \qquad (24)$$

where $\delta = J_{x+y} - (4\ln 2)J_0$. Expression (24) can give a satisfactory approximation when the value of $|\delta|$ is not near $4J_0$. The exact critical field H_{c3} for the third QPT is the same as H_{c2} in (11). When the example in Figure 8 has numerical points $H_{c1} = 4.244J_0$ and $H_{c2} = 4.928J_0$, the expressions (21) and (24) provide the analytic results $H_{c1} = 4.256J_0$ and $H_{c2} = 4.924J_0$.

In the Bethe ansatz energy (6), the one-particle legpart energy is $\varepsilon = -J_0/(\mu^2 + 1/4)$, which can also be transformed into a dispersion $\varepsilon(k) = J_0(2\cos k - 2)$ when the wave vector $e^{ik} = (\mu - i/2)/(\mu + i/2)$ is used. The part under the Fermi surface decides the proportion (particle number) of the component in the GS. When a component enters or gets out of the GS, the round bottom of the dispersion will result in a quick change in the proportion of the corresponding component. Therefore, singular behavior can be observed at the QPT's, including the cusp singularities [42,43], though the details of the singularity behavior are also influenced by the field-energy dependence

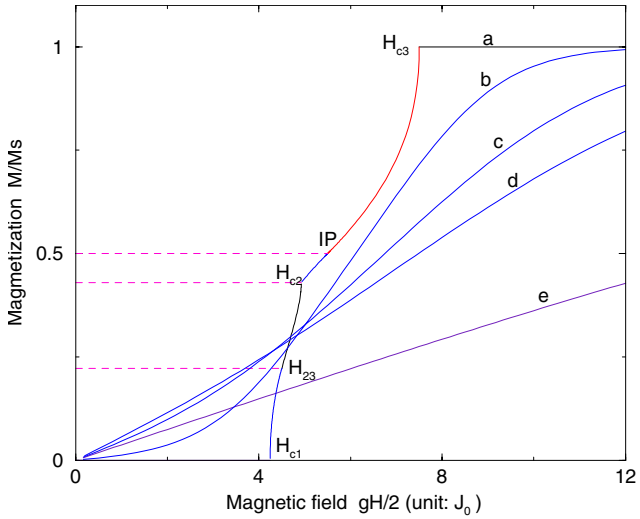

Fig. 8. Magnetizations in the z direction for a two-component gapped ladder case, $J_x = J_y = 2J_0$, $J_z = 20J_0$. The curves a, b, c, d and e are plotted for different temperatures, $T = 0$, $2J_0$, $4J_0$, $6J_0$ and $20J_0$, respectively. In the gapped phase $H < H_{c1}$, two components φ_1 and φ_2 are involved in the ground state (GS) ($T = 0$). The component φ_3 begins to enter the GS at the critical point H_{c1}, and reaches the same energy as φ_2 at H_{23}. The component φ_2 gets out of the GS at the second critical field H_{c2}. The magnetization curves for different temperatures do not go through the IP as in the one-component gapped ladder case. When the field is applied in the x- or y-direction, the GS magnetization will increase from the beginning due to the gapless excitation in these directions.

and the structures of the Fermi seas at the critical point. The phase between H_{c1} and H_{c2} has three components in the GS, which involves an SU(3) Bethe ansatz since the other component is not involved in the GS. Despite some different details due to the field-energy dependence, the cusp singularity is similar to the SU(3) spin chain [42], as one can see from curve (a) of the example in Figure 8.

The IP in the one-component gapped ladder case will not be invariant in the two-component ladder case. If the component φ_2 gets out of the GS after H_{IP}, φ_2 is gapless. Although the components φ_1 and φ_3 still have the same proportion at the IP, any small temperature will excite more components of φ_2 and consequently decreases the proportion of φ_1 and φ_3. Therefore, the temperature will lower the total magnetization from that of the GS. If the component φ_2 gets out of the GS before H_{IP}, given the condition (23), the IP can hardly be invariant. Despite the existence of a gap in excitations of φ_2 at H_{IP}, the gap is actually quite small

$$\Delta_{IP2} < (4 - \ln 2)J_0, \qquad (25)$$

relative to the strong rung interaction. Thus a low temperature of order J_0 will still stimulate considerable excitations to φ_2, and lower the magnetization at H_{IP}. We illustrate this by the example in Figure 8.

5 Summary

We have introduced a two-leg spin-1/2 ladder with a general anisotropic XYZ rung interaction. In particular, the exact rung state basis for this model was found. We have studied the effect of the anisotropic rung interaction by solving the integrable ladder in the context of the thermodynamic Bethe ansatz and the high-temperature expansion. Two kinds of gapped ladders were provided, involving one and two components, respectively, in the groundstate in the absence of the magnetic field. We have analytically obtained all the corresponding critical fields for the field-induced quantum phase transitions. The magnetizations and susceptibilities in different directions separate under the rung anisotropy. The magnetization inflection point is lowered from the half-saturation, and a weak change in magnetization still remains after the last quantum phase transition. The inflection point in the two-component gapped ladder case is not invariant as in the one-component gapped ladder case, due to field-induced three-component competition or small excitation gap.

We thank Huan-Qiang Zhou and Xi-Wen Guan for helpful discussions. ZJY thanks FAPERJ and FAPERGS for financial support. IR thanks PRONEX and CNPq. AF thanks FAPERGS and CNPq. BC is supported by National Nature Science Foundation of China under Grant No.10274070 and Zhejiang Natural Science Foundation RC02068.

References

1. E. Dagotto, T.M. Rice, Science **271**, 618 (1996); E. Dagotto, Rep. Prog. Phys. **62**, 1525 (1999)
2. M. Azuma, Z. Hiroi, M. Takano, K. Ishida, Y. Kitaoka, Phys. Rev. Lett. **73**, 3463 (1994)
3. G. Chaboussant, P.A. Crowell, L.P. Lévy, O. Piovesana, A. Madouri, D. Mailly, Phys. Rev. B **55**, 3046 (1997)
4. C.P. Landee, M.M. Turnbull, C. Galeriu, J. Giantsidis, F.M. Woodward, Phys. Rev. B **63**, 100402 (2001)
5. B.C. Watson, V.N. Kotov, M.W. Meisel, D.W. Hall, G.E. Granroth, W.T. Montfrooij, S.E. Nagler, D.A Jensen, R. Backov, M.A. Petruska, G.E. Fanucci, D.R. Talham, Phys. Rev. Lett. **86**, 5168 (2001)
6. T. Yildirim, A.B. Harris, O. Entin-Wohlman, A. Aharony, Phys. Rev. Lett. **73**, 2919 (1994)
7. J. Stein, O. Entin-Wohlman, A. Aharony, Phys. Rev. B **53**, 775 (1996)
8. T. Moriya, Phys. Rev. **120**, 91 (1960); J. Stein, Phys. Rev. B **53**, 785 (1996)
9. V. Kiryukhin, Y.J. Kim, K.J. Thomas, F.C. Chou, R.W. Erwin, Q. Huang, M.A. Kastner, R.J. Birgeneau, Phys. Rev. B **63**, 144418 (2001)
10. V.Yu. Yushankhai, R. Hayn, Europhys. Lett. **47**, 116 (1999)
11. V. Kataev, K.-Y. Choi, M. Grüninger, U. Ammerahl, B. Büchner, A. Freimuth, A. Revcolevschi, Physica B **312-313**, 614 (2002)
12. R. Citro, E. Orignac, Phys. Rev. B **65**, 134413 (2002)
13. S. Cai, J. Dai, Y. Wang, Phys. Rev. B **66**, 134403 (2002)
14. B.R. Patyal, B.L. Scott, R.D. Willett, Phys. Rev. B **41**, 1657 (1990)
15. C.A. Hayward, D. Poilblanc, L.P. Lévy, Phys. Rev. B **54**, 12649 (1996)
16. X.-Q. Wang, L. Yu, Phys. Rev. Lett. **84**, 5399 (2000)
17. D.C. Johnston, M. Troyer, S. Miyahara, D. Lidsky, K. Ueda, M. Azuma, Z. Hiroi, M. Takano, M. Isobe, Y. Ueda, M.A. Korotin, V.I. Anisimov, A.V. Mahajan, L.L. Miller, `cond-mat/0001147`
18. Q. Gu, D.-K. Yu, J.-L. Shen, Phys. Rev. B **60**, 3009 (1999)
19. R. Chitra, T. Giamarchi, Phys. Rev. B **55**, 5816 (1997)
20. F. Mila, Eur. Phys. J. B **6**, 201 (1998)
21. Y. Wang, Phys. Rev. B **60**, 9236 (1999)
22. M.T. Batchelor, X.-W. Guan, N. Oelkers, K. Sakai, Z. Tsuboi, A. Foerster, Phys. Rev. Lett. **91**, 217202 (2003)
23. M.T. Batchelor, X.W. Guan, A. Foerster, H.Q. Zhou, New J. Phys. **5**, 107 (2003)
24. Z.-J. Ying, I. Roditi, H.-Q. Zhou,`cond-mat/0405274`
25. Y.Q. Li, M. Ma, D.N. Shi, F.C. Zhang, Phys. Rev. Lett. **81**, 3527 (1998)
26. Y.Q. Li, M. Ma, D.N. Shi, F.C. Zhang, Phys. Rev. B **60**, 12781 (1999)
27. S.-J. Gu, Y.-Q. Li, H.-Q. Zhou, Phys. Rev. B **69**, 144405 (2004)
28. Z.J. Ying, A. Foerster, X.W. Guan, B. Chen, I. Roditi, Eur. Phys. J. B **38**, 535 (2004)
29. C.N. Yang, C.P. Yang, J. Math. Phys. **10**, 1115 (1969)
30. H. Frahm, V.E. Korepin, Phys. Rev. B **42**, 10553 (1990)
31. Z. Tsuboi, J. Phys. A **36**, 1493 (2003)
32. M. Shiroishi, M. Takahashi, Phys. Rev. Lett. **89**, 117201 (2002)
33. B. Sutherland, Phys. Rev. B **12**, 3795 (1975)
34. M. Takahashi, Prog. Theor. Phys. **46**, 401 (1971)
35. A. Kuniba, T. Nakanishi, J. Suzuki, Int. J. Mod. Phys. A **9**, 5215 (1994)
36. M. Suzuki, Phys. Rev. B **31**, 2957 (1985); A. Klümper, Ann. Phys. (Leipzig) **1**, 540 (1992); G. Jüttner, A. Klümper, J. Suzuki, Nucl. Phys. B **487**, 650 (1997)
37. T. Barnes, E. Dagotto, J. Riera, E.S. Swanson, Phys. Rev. B **47**, 3196 (1993)
38. M. Reigrotzki, H. Tsunetsugu, T.M. Rice, J. Phys.: Condens. Matter **6**, 9235 (1994)
39. Zheng Weihong, V. Kotov, J. Oitmaa, Phys. Rev. B **57**, 11439 (1998)
40. I. Affleck, Phys. Rev. B **43**, 3215 (1991)
41. M.G. Krein Usp. Mat. Nauk **13**, 3 (1958)
42. J.B. Parkinson, J. Phys.: Condens. Matter **1**, 6709 (1989)
43. H. Kiwata, Y. Akutsu, J. Phys. Soc. Jpn **63**, 4269 (1994); K. Okunishi, Prog. Theor. Phys. Supp. **145**, 119 (2002)